Processing and Application of Ceramics 14 [2] (2020) 134–140
https://doi.org/10.2298/PAC2002134D

Microstructure, XRD and Mössbauer spectroscopy study of Gd doped $BiFeO_3$

Jolanta Dzik[1,*], Tomasz Pikula[2], Diana Szalbot[1], Małgorzata Adamczyk-Habrajska[1], Beata Wodecka-Duś[1], Rafał Panek[3]

[1]*University of Silesia, Faculty of Science and Technology, Institute of Materials Engineering, 12, Zytnia Str., 41-200 Sosnowiec, Poland*
[2]*Lublin University of Technology, Institute of Electronics and Information Technology, 38A Nadbystrzycka Str., 20-618 Lublin, Poland*
[3]*Lublin University of Technology, Faculty of Civil Engineering and Architecture, Department of Geotechnical Engineering, 40 Nadbystrzycka Str., 20-618 Lublin, Poland*

Received 20 November 2019; Received in revised form 25 February 2020; Accepted 2 April 2020

Abstract

The results of fabrication process and characterization of $Bi_{1-x}Gd_xFeO_3$ (x = 0.05, 0.07, 0.10) ceramics are reported in the paper. The samples were prepared by standard solid state reaction method from the mixture of oxides: Bi_2O_3, Fe_2O_3 and Gd_2O_3. The influence of Gd substitution on the microstructure and density of $Bi_{1-x}Gd_xFeO_3$ was studied. Phase composition and structure of the obtained samples were investigated by X-ray diffraction. It turns out that the $Bi_{1-x}Gd_xFeO_3$ solid solutions with x = 0.05 and 0.07 crystallize in trigonal structure characteristic of $BiFeO_3$ compound. For the sample with x = 0.1, beside the major trigonal phase, 6% of orthorhombic phase typical for $GdFeO_3$ was detected. Hyperfine interaction parameters were studied by Mössbauer spectroscopy. Mössbauer results proved that the spin cycloid characteristic of $BiFeO_3$ compound gradually disappears when substituting Gd^{3+} ions at the Bi^{3+} sites.

Keywords: *$BiFeO_3$, Gd^{3+} doping, solid state method, X-ray diffraction, Mössbauer spectroscopy*

I. Introduction

Multiferroics are the class of materials that possess at least two of the properties among ferroelectricity, ferromagnetism and ferroelasticity in the same phase [1,2]. The magnetoelectric coupling between magnetic and electrical orders in these multiferroics enables to control magnetic polarization by applying electric field and vice versa [3]. Multiferroic materials attract particular interest in view of both fundamental physics and realizing multifunctional devices used in information storage, spintronics, sensors and other fields [4,5].

Bismuth ferrite $BiFeO_3$ is one of the widely studied materials which exhibits ferroelectric and antiferromagnetic properties at room temperature in the same phase. Bismuth ferrite has high Curie ($T_C \approx 1103$ K) and Néel ($T_N \approx 643$ K) temperatures [6,7]. The crystal structure of bismuth ferrite is described by the rhombohedral space group *R*3*c*, which allows antiphase octahedral tilting and ionic displacements from the centrosymmetric positions along the $[001]_H$ direction [8]. As it is well known, bismuth ferrite is a G-type antiferromagnet due to superexchange interaction of neighbouring Fe^{3+} ions [9]. Each Fe^{3+} ion is located inside oxygen octahedron. In the second coordination sphere there is 8 Bi^{3+} ions while the third sphere is occupied by 6 Fe^{3+} ions with spins antiparallel with respect to the spin of the central Fe^{3+} ion. In fact, magnetic moments of two neighbouring Fe^{3+} ions are not strictly antiparallel but they are canted due to the Dzialoshynskii-Moriya interaction [10]. Thus, week ferromagnetic moment arising from incomplete compensation of sublattices should appear. However, there is spin cycloid with period of 620 Å superimposed on the canted antiferromagnetic order which cancels out the weak ferromagnetic moment [7].

* Corresponding author: tel: +48 32 2691857,
e-mail: *jolanta.dzik@us.edu.pl*

There is a lot of scientific research available on $BiFeO_3$ based materials. Lomanova *et al.* [11] reported the possibility of $Bi_2Fe_4O_9$ and $Bi_{25}FeO_{39}$ formation during $BiFeO_3$ synthesis and this was shown to be dependent upon the quality of the initial reagents. In recent years, many attempts have been made to modify the structure of $BiFeO_3$ by suitable substitution of some rare earth ions. Doping of $BiFeO_3$ with rare earth ions at A-site proved to be an effective way to improve its ferroelectric properties [12,13] as well as A-site doping with ions of smaller radius influencing the Fe–O–Fe bond angle, giving a more insulating character to bismuth ferrite [14,15]. Doping of B-site is also another effective way to reduce the leakage current in $BiFeO_3$ and to improve its multiferroic properties [16,17].

In this paper, Gd-doped $BiFeO_3$ ceramics were synthesized by solid-state reaction method. Microstructure and chemical composition tests were carried out using a scanning electron microscope. Investigations of microstructure, crystalline structure and magnetic properties of the obtained materials were performed using X-ray diffraction (XRD) and ^{57}Fe Mössbauer spectroscopy (MS).

II. Experimental procedure

Gd-doped $BiFeO_3$ powders having the formula $Bi_{1-x}Gd_xFeO_3$ (x = 0.05, 0.07, 0.10) were prepared by the conventional solid state reaction route. High purity Bi_2O_3, Fe_2O_3 and Gd_2O_3 (99.99%) powders were weighed according to the stoichiometry, mixed and milled in a planetary mill for t = 24 h with zirconia-yttria balls (ZrO_2-Y_2O_3, with the diameter of d = 10 mm) in polyamide cup containing ethyl alcohol (Poch, 96%). In the next step, the ground and dried powders were uniaxially cold pressed by a hydraulic press at P = 60 MPa in a steel matrix into disks with a diameter of d = 23 mm. The compacts were placed in corundum crucibles, stacked and separated from each other with Al_2O_3 alumina ballast (Poch, 99.9%) so that they did not touch the crucible and each other. The samples were heated using temperature rate of 5 °C/min up to T = 800 °C for t = 3 h. The temperature and duration of the reaction were determined as the optimal conditions for gadolinium doped bismuth ferrite, resulting in the densest $Bi_{1-x}Gd_xFeO_3$ samples with the lowest content of secondary phases. The solid-phase reaction that occurs during the synthesis can be written by the following equation:

$$\frac{1-x}{2}Bi_2O_3+\frac{x}{2}Gd_2O_3+\frac{1}{2}Fe_2O_3\rightarrow Bi_{1-x}Gd_xFeO_3 \quad (1)$$

After synthesis, the compacts were placed in a porcelain mortar and ground thoroughly. The pre-ground powders were again milled with zirconia-yttria balls in a planetary mill for t = 24 h in polyamide containers containing ethyl alcohol. After drying the powders were pressed into discs d = 10 mm in diameter, at pressure of

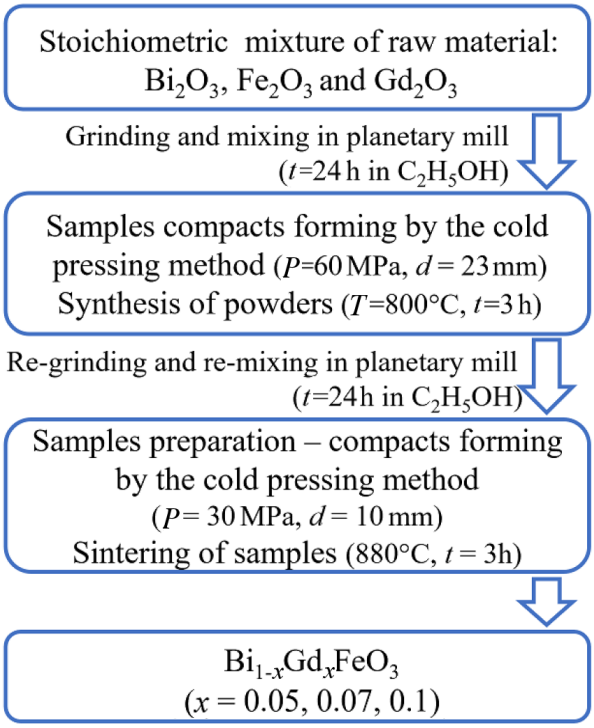

Figure 1. The flowchart of the fabrication process of $Bi_{1-x}Gd_xFeO_3$ ceramics

P = 30 MPa. Air sintering was carried out at T = 880 °C for t = 3 h. The whole process is schematically presented in Fig. 1.

The microstructure and chemical composition of the final ceramics were examined with a scanning electron microscope (SEM, JSM - 7100F) operating at 15 kV and equipped with an energy dispersive spectrometer (EDS, NORAN Vantage). EDS spectrum, which is dependent on the number of counts as a function of radiation, makes it possible to identify the elements contained in the tested material. The density of the obtained ceramics was calculated from the geometry and the mass of the sample.

X-ray diffraction measurements were made on a X'Pert Pro diffractometer. A Cu-Kα X-ray wavelength λ = 0.154 nm was used. Phase and structural analyses of the X-ray diffraction patterns of $Bi_{1-x}Gd_xFeO_3$ powders were carried out using HighScore Plus program equipped with PDF2 crystallographic database.

The samples were also analysed using Mössbauer spectroscopy. A POLON spectrometer working in range utilization mode was used. As a source of gamma quanta with energy E = 14.4 keV, ^{57}Co nuclei embedded in the Rh crystal matrix were used.

III. Results and discussion

XRD patterns of the $Bi_{1-x}Gd_xFeO_3$ solid solutions are shown in Fig. 2. Phase analysis of the diffractograms revealed that beside the major $BiFeO_3$-like phase small amounts of parasitic $Bi_2Fe_4O_9$ and $Bi_{25}FeO_{40}$ phases exist. The most intensive peaks from these phases were

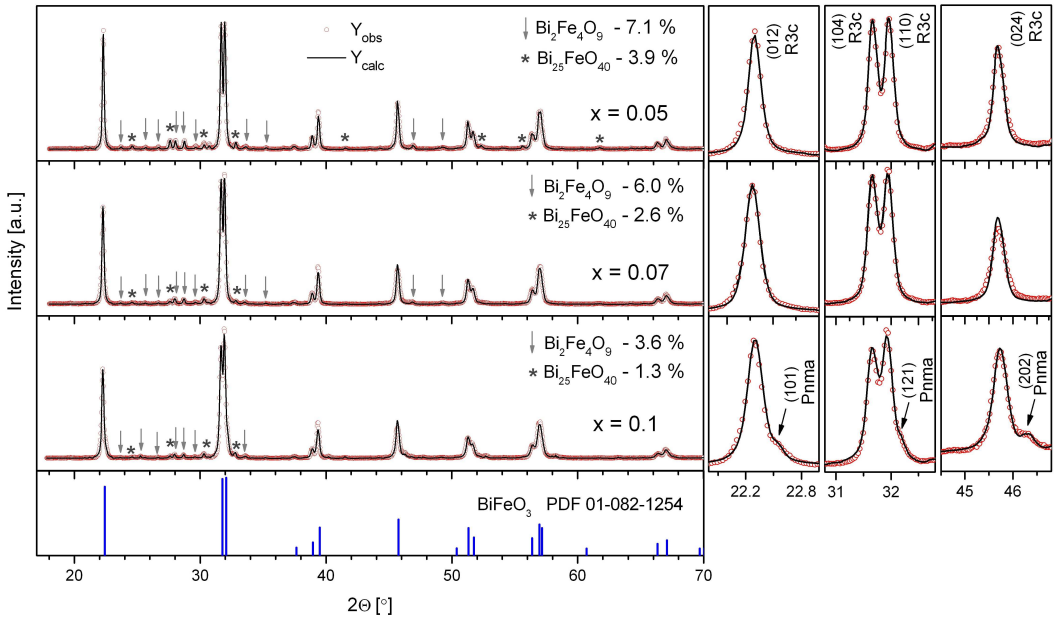

Figure 2. XRD patterns of $Bi_{1-x}Gd_xFeO_3$ solid solutions (together with the standard pattern for undoped $BiFeO_3$ sample). The right panel shows enlargement of the most intense peaks in the vicinity of 2θ = 22.5°, 32° and 46°

marked in Fig. 2. It can be seen that the smallest contribution of parasitic phases was observed for the sample with x = 0.1. The diffractograms were numerically fitted by the Rietveld refinement method. The best fit was achieved assuming trigonal crystal system (space group *R*3*c* of rhombohedral lattice system) for the $Bi_{1-x}Gd_xFeO_3$ solid solutions. The quantitative phase analysis showed that the content of the major $BiFeO_3$ phase is 89.0, 91.4 and 95.1 wt.% for x = 0.05, x = 0.07 and x = 0.10, respectively. However, in the case of the sample with x = 0.1 small amount (6 wt.%) of orthorhombic *Pnma* phase characteristic of $GdFeO_3$ compound was detected. This can be evidenced e.g. by appearance of small peaks in the vicinity of 2θ = 22.5°, 32.1° and 46.3° of 2θ angle (see the right panel in Fig. 2) which correspond to the (101), (121) and (202) plains of *Pnma* structure. Thus, it may be supposed that the gradual transformation from *R*3*c* to *Pnma* structure starts for about 10% of Gd-doping of $BiFeO_3$. This result agrees well with data published by Guo *et al.* [18]. They revealed 11.1% of orthorhombic *Pnma* phase and 88.9% of *R*3*c* phase for the $Bi_{0.9}Gd_{0.1}FeO_3$ solid solution prepared by sol-gel method. It was shown by Ablat *et al.* [19] that single *Pnma* phase was obtained for $x > 0.15$ when the samples were prepared by solid state reaction method. The detailed structural parameters derived from the Rietvled refinement of XRD patterns are summarized in Table 1. The data for the undoped $BiFeO_3$ taken from Ref. [20] were included for comparison. Gradual decrease of lattice parameters a, b, c and the volume of unit cell, V, can be clearly observed. This is the result of partial substitution of larger Bi^{3+} ions (ionic radius in VIII coordination r_{Bi} = 1.17 Å) by smaller Gd^{3+} ions (r_{Gd} = 1.053 Å in VIII coordination) [1].

SEM micrographs of the $Bi_{1-x}Gd_xFeO_3$ ceramics are shown in Fig. 3. The procedure of recording sample images was random selection of fields distributed over the entire surface of the tested ceramics. The microstructure is characterized by a compact, non-porous structure with well-developed grains. A slight increase in grain size is visible along with the increase in gadolinium concentration in the obtained materials.

Based on the density studies, it can be stated that the increase in gadolinium concentration resulted in decreased density, which are as follows: 7.353, 7.028 and 6.712 g/cm^3 for the $Bi_{0.95}Gd_{0.05}FeO_3$, $Bi_{0.93}Gd_{0.07}FeO_3$ and $Bi_{0.9}Gd_{0.1}FeO_3$ ceramics, respectively.

EDS spectra of the $Bi_{1-x}Gd_xFeO_3$ ceramics are shown in Fig. 4 and the theoretical and experimental contents of elements (calculation for simple oxides) are given in Table 2. The results prove that the chemical composition of the produced ceramics has been preserved.

Table 1. Structural parameters of $Bi_{1-x}Gd_xFeO_3$ derived from the Rietveld refinement of XRD patterns (*A* denotes relative content of a phase)

Sample	Crystal system	Space group	a [Å]	b [Å]	c [Å]	V [Å^3]	A [wt.%]
$BiFeO_3$ [21]	Trigonal (hex. axes)	*R*3*c*	5.578		13.862	373.4	-
$Bi_{0.95}Gd_{0.05}FeO_3$	Trigonal (hex. axes)	*R*3*c*	5.570		13.830	371.6	89
$Bi_{0.93}Gd_{0.07}FeO_3$	Trigonal (hex. axes)	*R*3*c*	5.566		13.814	370.6	91.4
$Bi_{0.9}Gd_{0.1}FeO_3$	Trigonal (hex. axes)	*R*3*c*	5.566		13.809	370.5	89
	Orthorhombic	*Pnma*	5.628	7.797	5.433	238.5	6

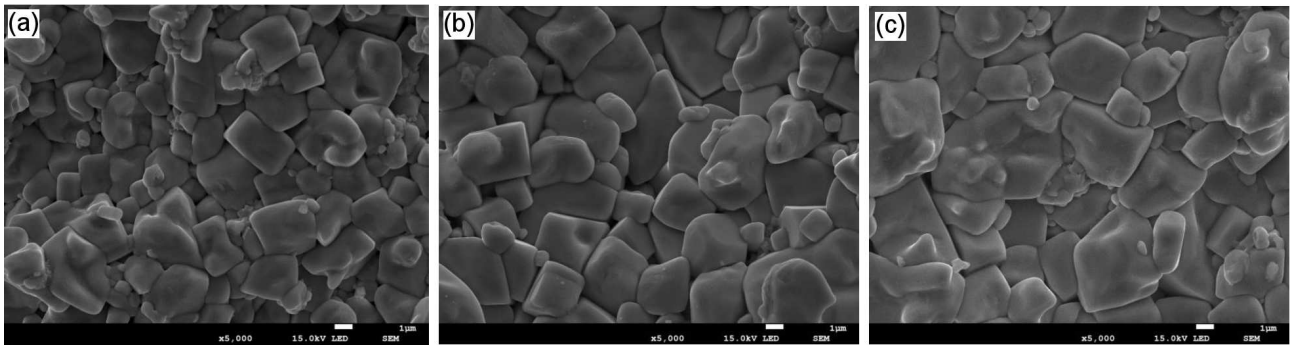

Figure 3. SEM micrographs of the fracture surface of sintered samples: a) $Bi_{0.95}Gd_{0.05}FeO_3$, b) $Bi_{0.93}Gd_{0.07}FeO_3$ and c) $Bi_{0.9}Gd_{0.1}FeO_3$

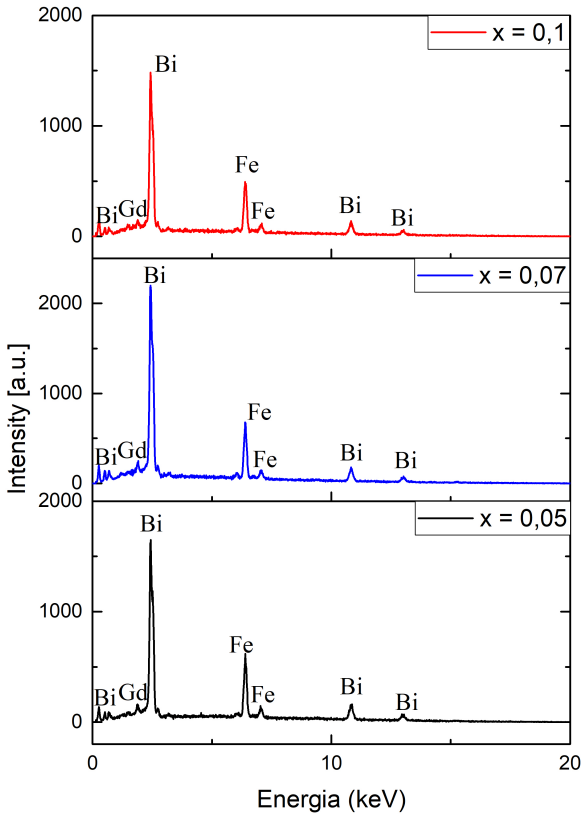

Figure 4. EDS spectra of $Bi_{1-x}Gd_xFeO_3$ ceramics

The measurement uncertainty is small and the largest discrepancy is ±3.58%. The EDS study confirmed both the quantitative and qualitative chemical composition of the produced $Bi_{1-x}Gd_xFeO_3$ ceramics. The analysis also showed the purity of the samples tested and excluded the presence of foreign elements and impurities.

Figure 5 shows room-temperature ^{57}Fe-Mössbauer spectra measured for the studied $Bi_{1-x}Gd_xFeO_3$ solid solutions. It is well known that ferro- and antiferromagnetic materials show six-line Mössbauer patterns (sextets) due to the Zeeman splitting of ^{57}Fe nuclear levels caused by the hyperfine magnetic field (HMF). On the other hand, paramagnetic phases show single line or doublet. Single line corresponds to the transition between excited nuclear state of 57Fe (spin I = 3/2) and ground state (spin I = 1/2). Doublet occurs when electric field gradient (EFG) is present at ^{57}Fe nucleus site [21]. As it can be seen in Fig. 5 the spectra consist of six-line part connected with antiferromagnetic $BiFeO_3$-like structure and small paramagnetic doublets D1 and D2 arising due to the parasitic $Bi_2Fe_4O_9$ and $Bi_{25}FeO_{40}$ phases. The total contribution of paramagnetic part to the whole spectrum is 17.5%, 11.5% and 8.3% for the samples with x = 0.05, 0.07 and 0.1, respectively. One can note that these are significantly higher values than the contributions derived from XRD patterns analysis: 11%, 8.6%, 4.9%. This can be explained in terms of different probabilities of recoilless absorption of 14.4 keV gamma radiation for the $Bi_{1-x}Gd_xFeO_3$ solid solution and parasitic phases. It is obvious that the probability will be higher for $Bi_2Fe_4O_9$ compound as it contains four Fe ions per formula unit (proportion of Fe and Bi ions 2:1) while the $Bi_{1-x}Gd_xFeO_3$ sample contains one Fe ion (proportion of Fe and Bi ions approximately 1:1).

Distortion in perovskite crystal structure occurs either through displacement of central cations from their centrosymmetric position or from the rotation of oxygen octahedral [22]. In $BiFeO_3$ both of them occur simultaneously leading to the lowering of the crystal symmetry from cubic to rhombohedral and break of inversion symmetry of perovskite cell. Oxygen octahedra rotates in the opposite way in adjacent chemical cells joint by the line along [111] pseudocubic direction which is also the direction of polarization vector P. Moreover, iron ions are displaced along the same polar [111] direction and

Table 2. Theoretical and experimental contents of elements (calculation for simple oxide) for $Bi_{1-x}Gd_xFeO_3$ ceramics

Sample	Content from EDS [%]			Theoretical content [%]			Content error [%]		
	Bi_2O_3	Gd_2O_3	Fe_2O_3	Bi_2O_3	Gd_2O_3	Fe_2O_3	Bi_2O_3	Gd_2O_3	Fe_2O_3
$Bi_{0.95}Gd_{0.05}FeO_3$	71.342	2.921	25.737	71.1	3.02	25.88	0.339	3.389	0.556
$Bi_{0.93}Gd_{0.07}FeO_3$	70.072	4.103	25.823	69.98	4.25	25.77	0.131	3.583	0.205
$Bi_{0.9}Gd_{0.1}FeO_3$	68.154	5.891	25.953	67.9	6.05	26.05	0.373	2.699	0.374

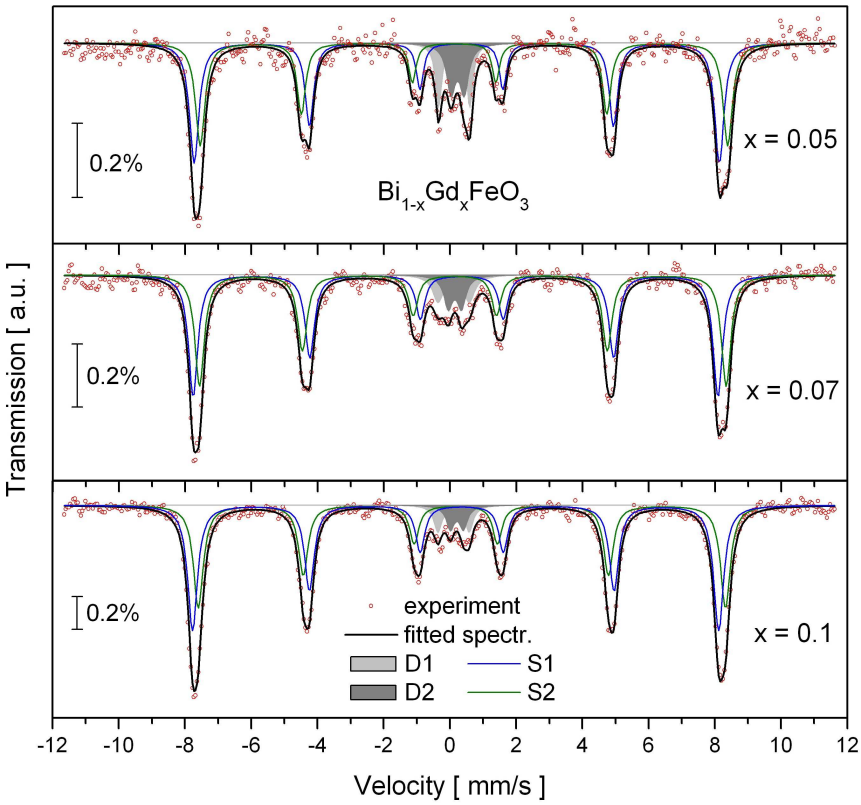

Figure 5. Mösbauer spectra measured for $Bi_{1-x}Gd_xFeO_3$ solid solutions. The components S1 and S2 come from $Bi_{1-x}Gd_xFeO_3$ solid solution and paramagnetic doublets D1 and D2 are due to $Bi_2Fe_4O_9$ and $Bi_{25}FeO_{40}$ parasitic phases

are off-centred with respect to the centre of oxygen octahedra [9]. The rotation of the octahedra and the iron ions displacement lead to differentiation of the iron-oxygen bond lengths. Thus, non-equivalent iron sites are generated with the local symmetry being lower than cubic causing creation of EFG at the Fe nuclei [23]. As a result, Mössbauer spectra of $BiFeO_3$ exhibit two overlapping sextets differing by both the hyperfine magnetic field, B_{hf}, and the electric field gradient reflected by quadrupole shift parameter 2ε. It is well documented in literature devoted to $BiFeO_3$ and rear earth-doped $BiFeO_3$ that satisfactory fit of Mösbauer spectrum can be achieved assuming two-sextet model [10,23–27]. Alternatively, more complicated models assuming B_{hf} values distribution as well as 2ε values distribution as a reflection of continuous change of the angle between B_{hf} vector and the axis of electric field gradient in spin cycloid have been applied [23,28–30]. In particular, Rusakov *et al.* [30] numerically simulated B_{hf} distribution for $BiFeO_3$ taking into account anharmonic cycloidal spin structure. They obtained so-called U-type B_{hf} distribution (sharp two peaks with well-defined two B_{hf} values). The two values of B_{hf} ($B_\perp$ and $B_\parallel$) were ascribed to two distinct (parallel and perpendicular to [111] direction) orientations of iron magnetic moments in spin cycloid. Pierzga *et al.* [23] compared both models and concluded that the two sextet model is a reasonable approximation of the models based on B_{hf} distribution.

The magnetic part of the spectra shown in Fig. 5 was fitted in approximation of two-sextet model (S1 and S2) as explained above. The derived hyperfine parameters are summarized in Table 3 and compared with the data obtained by other authors for the undoped $BiFeO_3$. The fitted sextets are characterized by two distinct B_{hf} values differing by ΔB_{hf} and two values of 2ε with opposite signs. This result is consistent with the data reported by others [24,28]. By analysing the shape of the magnetic part of the spectra one can note two effects: asymmetry of the spectra reflected by different amplitudes of 1st and 6th line (see parameter ΔA_{16} in Table 3) and inhomogeneous lines broadening (e.g. different widths of lines Γ_1 and Γ_6). As widely discussed in Ref. [31] the line broadenings and spectral asymmetry in the spiral magnetic phase of $BiFeO_3$ are due to different causes: the broadenings arise from the slight modulation of the hyperfine energies as the magnetic moment rotates with respect to the principal axis of the EFG tensor, and the asymmetry stems from an intrinsic anisotropy of the magnetic hyperfine interaction at a site with trigonal symmetry. Thus, the spectra presented in Fig. 5 confirm existence of cycloidal spin ordering in the studied samples. The increase of the Gd dopant concentration leads to the reduction of the spectra asymmetry as evidenced by the drop of ΔA_{16} parameter and disappearance of inhomogeneous lines broadening (Γ_1 and Γ_6 much different for the sample with $x = 0.05$, but comparable for the sample with $x = 0.1$). Moreover, the difference between the

Table 3. Results of Mössbauer spectra fitting for $Bi_{1-x}Gd_xFeO_3$ solid solutions (δ - isomer shift, 2ε - quadrupole shift, B_{hf} - hyperfine magnetic field, $\Delta B_{hf} = B_{S2} - B_{S1}$ - difference of B_{hf} for S1 and S2 components, C - contribution to the total spectrum, Γ_1, Γ_6 - full width of the 1st and 6th absorption line, ΔA_{16} - asymmetry of the magnetic part of the spectrum expressed as relative difference of line 1 and line 6 amplitudes). The data for the undoped $BiFeO_3$ from the literature [24,27,28] were included for comparison.

Sample	Component	δ [mm/s]	2ε [mm/s]	B_{hf} [T]	ΔB_{hf} [T]	C [%]	Γ_1 [mm/s]	Γ_6 [mm/s]	ΔA_{16} [%]	
$BiFeO_3$ [24]	S1	0.39	−0.12	49.47	0.37	-	-	-	-	-
	S2	0.39	0.32	49.84		-				
$BiFeO_3$ [28]	S1	-	−0.097	49.58	0.35	-	-	-	-	29.2
	S2	-	0.343	49.93		-				
$BiFeO_3$ [27]	S1	0.38	0.09	49.42	0.33	47.2	100	0.43	0.58	20
	S2	0.41	0.19	49.75		52.8				
$Bi_{0.95}Gd_{0.05}FeO_3$	S1	0.37	−0.15	49.36	0.22	44.4	82.5	0.48	0.59	16.6
	S2	0.37	0.29	49.58		38.1				
$Bi_{0.93}Gd_{0.07}FeO_3$	S1	0.37	−0.18	49.32	0.17	46.2	88.5	0.47	0.54	12.3
	S2	0.36	0.24	49.49		42.3				
$Bi_{0.9}Gd_{0.1}FeO_3$	S1	0.37	−0.18	49.44	0.09	50.4	91.7	0.47	0.49	6.3
	S2	0.37	0.19	49.53		41.3				

HMF fields of the two sextets, ΔB_{hf}, significantly decreases reaching as little as 0.09 T for the sample with $x = 0.1$. Hence, we conclude that the increasing amount of Gd in the structure of $BiFeO_3$ causes gradual destruction of spin cycloid as proved by disappearance of inhomogeneous lines broadening. Besides, the reduction of spectral asymmetry ΔA_{16} and drop of the difference between two values of HMF, ΔB_{hf}, can be accounted for structural changes in the rhombohedral lattice. It can be supposed that increase of Gd concentration causes change of distortion of FeO_6 octahedral structure thus, the two iron sites become more equivalent as evidenced by the drop of ΔB_{hf}. This conclusion is supported by findings of Xiao *et al.* [27], although it needs further investigations. The values of isomer shift δ (~0.37 mm/s) confirm that only trivalent iron ions in high spin state are present in the structure of $Bi_{1-x}Gd_xFeO_3$.

IV. Conclusions

Conventional solid state reaction route and sintering at 880 °C were successfully adopted for preparation of $Bi_{1-x}Gd_xFeO_3$ (for x = 0, 0.05, 0.07, 0,1) ceramics. An addition of gadolinium affects the grain size and causes a slight increase in grains in the materials obtained. XRD studies revealed that the $Bi_{1-x}Gd_xFeO_3$ solid solutions with $x = 0.05$ and 0.07 have rhombohedral *R*3*c* structure characteristic of $BiFeO_3$ compound. For the sample with $x = 0.1$, beside the major *R*3*c* phase, 6% of orthorhombic *Pnma* phase characteristic of $GdFeO_3$ compound was detected. It was shown that increase of Gd dopant concentration leads to the reduction of unit cell volume. Mössbauer spectroscopy was applied for investigation of hyperfine interaction parameters of the samples and confirmed phase composition deduced from XRD patterns analysis. Mössbauer investigations proved that the studied solid solutions exhibit aniferromagnetic $BiFeO_3$-like magnetic structure with cycloidal modulation of spins arrangement. Substitution of increasing amounts of Gd^{3+} ions causes systematic change of FeO_6 octahedral distortion and gradual destruction of the spin cycloid.

References

1. D. Khomskii, "Classifying multiferroics: Mechanisms and effects", *Physics*, **2** (20) (2009) 1–8.
2. H. Singh, A. Kumar, K.L. Yadav, "Structural, dielectric, magnetic, magnetodielectric and impedance spectroscopic studies of multiferroic $BiFeO_3$-$BaTiO_3$ ceramics", *Mater. Sci. Eng. B*, **176** (2011) 540–547.
3. N.A. Hill, "Why are there so few magnetic ferroelectrics?", *J. Phys. Chem. B*, **104** [29] (2000) 6694–6709.
4. V.A. Khomchenko, D.A. Kiselev, I.K. Bdikin, V.V. Shvartsman, P. Borisov, W. Kleemann, J.M. Vieira, A.L. Kholkin, "Crystal structure and multiferroic properties of Gd-substituted $BiFeO_3$", *Appl. Phys. Lett.*, **93** (2008) 262905.
5. M. Fiebig, "Revival of the magnetoelectric effect", *J Phys. D Appl. Phys.*, **38** (2005) 123–152.
6. J.B. Neaton, C. Ederer, U.V. Waghmare, N.A. Spaldin, K.M. Rabe, "First-principles study of spontaneous polarization in multiferroic $BiFeO_3$", *Phys. Rev. B*, **71** (2005) 014113–014121.
7. I. Sosnowska, T. Peterlin-Neumaier, E. Steichele, "Spiral magnetic ordering in bismuth ferrite", *J. Phys. C Solid State Phys.*, **15** (1982) 4835–4846.
8. M. Arora, S. Chauhan, P.C. Sati Manoj, K. Sandeep Chhoker, "Evidence of spin-two phonon coupling and improved multiferroic behavior of $Bi_{1-x}Dy_xFeO_3$ nanoparticles", *Ceram. Int.*, **40** [Part B] (2014) 13347–13356.
9. G. Catalan, J.F. Scott, "Physics and applications of bismuth ferrite", *Adv. Mater.*, **21** (2009) 2463–2485.
10. C. Blaauw, F. van der Woude, "Magnetic and structural properties of $BiFeO_3$", *J. Phys. C Solid State*, **6** (1973) 1422–1431.
11. N.A. Lomanova, V.V. Gusarov, "Influence of synthesis temperature on $BiFeO_3$ nanoparticles formation",

Nanosyst. Phys. Chem. Mat., **4** [5] (2013) 696–705.
12. S.B. Emery, C.J. Cheng, D. Kan, F.J. Rueckert, S.P. Alpay, V. Nagarajan, I. Takeuchi, B.O. Wells, "Phase coexistence near a morphotropic phase boundary in Sm-doped $BiFeO_3$ films", *Appl. Phys. Lett.*, **97** (2010) 152902–152915.
13. G.L. Yuan, S. Wing Or, J.M. Liu, Z.G. Liu, "Structural transformation and ferroelectromagnetic behavior in single-phase $Bi_{1-x}Nd_xFeO_3$ multiferroic ceramics", *Appl. Phys. Lett.*, **89** (2006) 052905–052909.
14. C.H. Yang, D. Kan, I. Takeuchi, V. Nagarajand, J. Seidel, "Doping $BiFeO_3$: approaches and enhanced functionality", *Phys. Chem. Chem. Phys.*, **14** (2012) 15953–15962.
15. J.H. Lee, H.J. Choi, D. Lee, M.G. Kim, C.W. Bark, S. Ryu, M.A. Oak, H.M. Jang, "Variations of ferroelectric off-centering distortion and 3d–4p orbital mixing in La-doped $BiFeO_3$ multiferroics", *Phys. Rev. B*, **82** (2010) 045113.
16. W. Liu, G. Tan, X. Xue, G. Dong, H. Ren, A. Xia, "Phase transition and enhanced multiferroic properties of (Sm, Mn and Cr) co-doped $BiFeO_3$ thin films", *Ceram. Int.*, **40** (2014) 12179–12185.
17. C.M. Raghavan, J.W. Kim, S.S. Kim, "Structural and ferroelectric properties of chemical solution deposited (Nd, Cu) co-doped $BiFeO_3$ thin film", *Ceram. Int.*, **39** (2013) 3563–3568.
18. R. Guo, L. Fang, W. Dong, F. Zheng, M. Shen, "Enhanced photocatalytic activity and ferromagnetism in Gd doped $BiFeO_3$ nanoparticles", *J. Phys. Chem. C*, **114** (2010) 21390–21396.
19. A. Ablat, R. Wu, M. Mamat, J. Li, E. Muhemmed, C. Si, R. Wu, J. Wang, H. Qian, K. Ibrahim, "Structural analysis and magnetic properties of Gd doped $BiFeO_3$ ceramics", *Ceram. Int.*, **40** (2014) 14083–14089.
20. I. Sosnowska, R. Przenioslo, P. Fischer, V.A. Murashov, "Investigation of crystal and magnetic structure of $BiFeO_3$ using neutron diffraction", *Acta Phys. Pol. A*, **86** (1994) 629–632.
21. G.K. Wertheim, *Mössbauer Effect: Principles and Applications*, Academic Press, New York, 1964.
22. F. Mumtaz, G.H. Jaffari, S.I. Shah, "Peculiar magnetism in Eu substituted $BiFeO_3$ and its correlation with local structure", *J. Phys. Condens. Matter*, **30** (2018) 435802.
23. A. Pierzga, A. Błachowski, K. Komędera, K. Ruebenbauer, A. Kalvane, R. Bujakiewicz-Korońska, "Orientation of the electric field gradient and ellipticity of the magnetic cycloid in multiferroic $BiFeO_3$", *Philos. Mag.*, **97** (2017) 168–174.
24. E. Jartych, A. Lisinska-Czekaj, D. Oleszak, D. Czekaj, "Comparative X-ray diffraction and Mössbauer spectroscopy studies of $BiFeO_3$ ceramics prepared by conventional solid-state reaction and mechanical activation", *Mater. Sci. Pol.*, **31** (2013) 211–220.
25. I.A. Santos, H.L.C. Grande, V.F. Freitas, L.F. Cotica, S.N. de Medeiros, A. Paesano Jr., E. Radovanovic, "Structural, microstructural and Mössbauer spectral study of the $BiFe_{1-x}Mn_xO_3$ mechanosynthesized system", *J. Non-Cryst. Solids*, **352** (2006) 1579–1584.
26. V.F. Freitas, H.L.C. Grande, S.N. de Medeiros, I.A. Santos, L.F. Cotica, A.A. Coelho, "Structural, microstructural and magnetic investigations in high-energy ball milled $BiFeO_3$ and $Bi_{0.95}Eu_{0.05}FeO_3$ powders", *J. Alloys Compd.*, **461** (2008) 48–52.
27. R.Z. Xiao, T. Hu, X.B. Yuan, J.J. Zhou, X.Q. Ma, D.J. Fu, "Studies of La- and Pr-driven reverse distortion of FeO_6 octahedral structure, magnetic properties and hyperfine interaction of $BiFeO_3$ powder", *RSC Adv.*, **8** (2018) 12060–12068.
28. A. Palewicz, T. Szumiata, R. Przeniosło, I. Sosnowska, I. Margiolaki, "Search for new modulations in the $BiFeO_3$ structure: SR diffraction and Mössbauer studies", *Solid State Commun.*, **140** (2006) 359–363.
29. J. Landers, S. Salamon, M. Escobar Castillo, D.C. Lupascu, H. Wende, "Mössbauer study of temperature-dependent cycloidal ordering in $BiFeO_3$ nanoparticles", *Nano Lett.*, **14** (2014) 6061–6065.
30. V. Rusakov, V. Pokatilov, A. Sigov, M. Matsnev, A. Pyatakov, "Temperature Mössbauer study of the spatial spin-modulated structure in the multiferroic $BiFeO_3$", *EPJ Web Conferences*, **185** (2018) 07010.
31. D. Lebeugle, D. Colson, A. Forget, M. Viret, P. Bonville, J.F. Marucco, S. Fusil, "Room-temperature coexistence of large electric polarization and magnetic order in $BiFeO_3$ single crystals", *Phys. Rev. B*, **76** (2007) 24116.